the FEBS Journal

Inter-flavin electron transfer in cytochrome P450 reductase – effects of solvent and pH identify hidden complexity in mechanism

Sibylle Brenner, Sam Hay, Andrew W. Munro and Nigel S. Scrutton

Manchester Interdisciplinary Biocentre and Faculty of Life Sciences, University of Manchester, UK

Keywords
electron transfer; pH dependence; redox potentiometry; (solvent) kinetic isotope effect; stopped-flow

Correspondence
N. S. Scrutton, Manchester Interdisciplinary Biocentre and Faculty of Life Sciences, University of Manchester, 131 Princess Street, Manchester M1 7DN, UK
Fax: +44 161 306 8918
Tel: +44 161 306 5152
E-mail: nigel.scrutton@manchester.ac.uk

(Received 4 June 2008, revised 8 July 2008, accepted 15 July 2008)

doi:10.1111/j.1742-4658.2008.06597.x

This study on human cytochrome P450 reductase (CPR) presents a comprehensive analysis of the thermodynamic and kinetic effects of pH and solvent on two- and four-electron reduction in this diflavin enzyme. pH-dependent redox potentiometry revealed that the thermodynamic equilibrium between various two-electron reduced enzyme species ($FMNH^{\bullet}$,$FADH^{\bullet}$; FMN,$FADH_2$; $FMNH_2$,FAD) is independent of pH. No shift from the blue, neutral di-semiquinone ($FMNH^{\bullet}$,$FADH^{\bullet}$) towards the red, anionic species is observed upon increasing the pH from 6.5 to 8.5. Spectrophotometric analysis of events following the mixing of oxidized CPR and NADPH (1 to 1) in a stopped-flow instrument demonstrates that the establishment of this thermodynamic equilibrium becomes a very slow process at elevated pH, indicative of a pH-gating mechanism. The final level of blue di-semiquinone formation is found to be pH independent. Stopped-flow experiments using excess NADPH over CPR provide evidence that both pH and solvent significantly influence the kinetic exposure of the blue di-semiquinone intermediate, yet the observed rate constants are essentially pH independent. Thus, the kinetic pH-gating mechanism under stoichiometric conditions is of no significant kinetic relevance for four-electron reduction, but rather modulates the observed semiquinone absorbance at 600 nm in a pH-dependent manner. The use of proton inventory experiments and primary kinetic isotope effects are described as kinetic tools to disentangle the intricate pH-dependent kinetic mechanism in CPR. Our analysis of the pH and isotope dependence in human CPR reveals previously hidden complexity in the mechanism of electron transfer in this complex flavoprotein.

Human cytochrome P450 reductase (CPR) belongs to a family of diflavin reductases that use the tightly bound cofactors FAD and FMN to catalyse electron transfer (ET) reactions [1–5]. Evolutionarily, human CPR (78 kDa) originated from a fusion of two ancestral genes encoding for a FMN-containing flavodoxin and a FAD-binding ferredoxin-$NADP^+$ reductase [2,3,6]. This is also reflected in its domain organization determined by X-ray crystallography of rat CPR, with the two flavin domains representing independent folding units that are linked by a flexible peptide hinge [7,8]. The natural electron donor of CPR NADPH, which binds near the FAD cofactor [8] and delivers two electron equivalents in the form of a hydride ion to the N5 of FAD [9,10]. CPR is bound to the endoplasmic reticulum by a hydrophobic N-terminal membrane anchor

Abbreviations
CPR, cytochrome P450 reductase; di-sq, di-semiquinone; ET, electron transfer; hq, hydroquinone; KIE, kinetic isotope effect; MSR, methionine synthase reductase; NHE, normal hydrogen electrode; NOS, nitric oxide synthase; ox, oxidized; PDA, photodiode array; QE, quasi-equilibrium; red, reduced; SKIE, solvent kinetic isotope effect; sq, semiquinone.

and mainly serves as an electron donor for the majority of the cytochrome P450 (P450) enzyme family members in the relevant organism [11–15]. Thus, the flavin cofactors mediate the successive transfer of two electrons from a two-electron donor, NADPH, to the obligatory one-electron acceptor moiety (the heme) in the P450s [16].

Selective removal of the flavin cofactors [4,17] and site-directed mutagenesis yielding FMN-deficient CPR [18] suggested that the physiological electron flow is given by NADPH → FAD → FMN → P450 heme, which was later substantiated by X-ray crystallographic studies of rat CPR protein [7,8]. Redox potentiometry conducted on both the full-length enzyme and the individual flavin domains of human CPR revealed reduction potentials of −66 mV (for the $FMN_{ox/sq}$ couple, E_1), −269 mV ($FMN_{sq/red}$, E_2), −283 mV ($FAD_{ox/sq}$, E_3) and −382 mV ($FAD_{sq/red}$, E_4), respectively, versus the normal hydrogen electrode (NHE) at pH 7.0 [19]. The relatively positive redox potential of the $FMN_{ox/sq}$ couple and the spectra obtained upon reduction of CPR provided an explanation for the greenish colour of the purified human enzyme, which could be assigned to the so-called 'air-stable' semiquinone (FMN_{sq} or $FMNH^{\bullet}$) with an intense absorbance maximum around 600 nm [4,5,20]. Formation of this neutral, 'blue' semiquinone, rather than the anionic, 'red' form ($FMN^{\bullet-}$, absorbance peak ~ 380 nm), has been attributed to a stabilizing hydrogen bond between the protonated N5 of the FMN and the carbonyl backbone of glycine 141 (G141) observed in the rat CPR crystal structure [8].

The kinetic mechanism of CPR has been extensively analysed, predominantly using steady-state assays with cytochrome *c* as a nonphysiological electron acceptor [16,21–28]. Thus, the observed kinetic parameters reflect both the reductive and oxidative half-reactions of the enzyme, resulting in a multitude of first- and second-order steps contributing to the observed k_{cat} and K_m values. To assist in the deconvolution of possible rate-limiting steps, pre-steady-state [29–31] and equilibrium perturbation techniques [32–34] have been used to study the reductive half-reaction in isolation, as shown schematically in Scheme 1. Hydride transfer from NADPH to the oxidized cofactor FAD (FAD_{ox}) yields the two-electron reduced FAD species, shown as protonated hydroquinone $FADH_2$ (abbreviated as FAD_{hq} or FAD_{red}). (Little is known about the actual protonation state of the hydroquinones, but they are most likely in an equilibrium mixture between protonated and deprotonated species [31].) Electrons are subsequently passed on to the FMN cofactor involving the intermediary formation of the so-called neutral di-semiquinone (di-sq)species of both flavins ($FMNH^{\bullet}$,$FADH^{\bullet}$ or $FMN_{sq}FAD_{sq}$) with an absorbance signature around 600 nm, yielding the formation of the thermodynamically favoured FMN hydroquinone ($FMNH_2$ or FMN_{hq}). The anionic sq species ($FMN^{\bullet-}$ and /or $FAD^{\bullet-}$; see above) have, to our knowledge, not been reported as an intermediate for the reductive half-reaction in CPR. Note that none of the three two-electron reduced species ($FMNH^{\bullet}$,$FADH^{\bullet}$; FMN,$FADH_2$; $FMNH_2$,FAD) is exclusively built up during the course of the reaction, but rather there is a (kinetic and/or thermodynamic) 'quasi-equilibrium' (QE) mixture of all states, as indicated by the [ ]. Binding of another NADPH molecule necessitates the dissociation of $NADP^+$, the time point of which is unknown, as indicated by the ( ) around $NADP^+$. The second hydride transfer from NADPH to FAD finally leads to the four-electron reduced enzyme, depicted as $FMNH_2$,$FADH_2$ (or $FMN_{red}FAD_{red}$).

Pre-steady-state data have been obtained by anaerobically mixing oxidized CPR with excess NADPH in a stopped-flow instrument and following either the decrease in absorbance at 450 nm indicative of flavin reduction or the formation and subsequent depletion of the neutral di-sq signal at 600 nm. Two main exponential phases were observed with the first reporting on the formation of the two-electron reduced enzyme species (~ $28 \cdot s^{-1}$ in rabbit CPR [31]; $20 \cdot s^{-1}$ in human

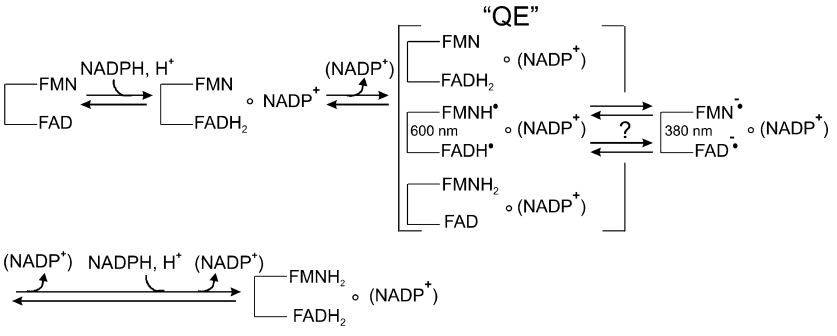

Scheme 1. Reductive half-reaction of human cytochrome P450 reductase.

CPR [30]) and the second on the four-electron reduction by a second molecule of NADPH (~ 5 and $\sim 3 \cdot s^{-1}$, respectively). The pre-steady-state data raised the question as to why the ET reaction catalysed by CPR is comparatively slow.

Structural evidence from $NADP^+$-bound rat CPR suggested that a tryptophan residue (Trp677 in rat, Trp676 in human CPR) stacks against the isoalloxazine ring of the FAD cofactor thereby preventing hydride transfer from NADPH to the flavin-N5 and thus necessitating a potentially rate-limiting conformational change [7]. The $NADP^+$-bound crystal structure also revealed an edge-to-edge distance for the flavin isoalloxazine C8 methyl carbons as short as 0.39 nm [8], which would be expected to result in a very fast and efficient ET between the flavin cofactors (up to $10^{10} \cdot s^{-1}$ using Dutton's ruler) [35–37]. However, temperature-jump (T-jump) relaxation experiments established that inter-flavin ET of NADPH-reduced human CPR occurs with an observed rate constant of $\sim 55 \cdot s^{-1}$, which has been attributed to domain movements prior to the actual ET [34]. Comparable rates were obtained in a laser flash photolysis, which yielded an inter-flavin ET rate from $FADH^\bullet$ to $FMNH^\bullet$ of $\sim 36 \cdot s^{-1}$ [38]. Product release and ligand binding steps have also been reported to rate-limit enzyme turnover under certain experimental conditions [13,24]. Further possible gating mechanisms include chemical gating, in which hydride transfer [24,27] and/or slow (de-)protonation steps (pH gating) become (partially) rate-limiting [39]. The latter might account for the apparently slow inter-flavin ET observed in the T-jump studies [34]; to our knowledge, this has never been analysed systematically under pre-steady-state conditions.

In this study, the stopped-flow technique was used to disentangle the complex kinetics associated with the two- and four-electron reduction of human CPR by addressing possible chemical and pH gating mechanisms. We were principally interested in the inter-flavin ET reactions, so the pH dependence of the kinetic behaviour at 600 nm was analysed, reporting on the formation of the blue, neutral sq species of the FMN and the FAD cofactors. Redox potentiometry at pH values ranging from 7 to 8.5 assisted in interpreting the observed solvent and primary kinetic isotope effects (SKIE and KIE, respectively).

Results

Reduction of CPR: photodiode array spectroscopy

Previous stopped-flow studies (see above) [30,31] have shown that a blue di-sq intermediate is formed when CPR is mixed with excess NADPH. Previous studies were typically performed at neutral pH and in this study we were interested in a possible pH-gating step, which might slow or even prevent the formation of this semiquinone (sq) species at elevated pH. In order to study the pH dependence of the reductive half-reaction kinetically, a constant ionic strength must be maintained, because the observed rate constants of CPR reduction have been found to significantly increase with the total ion concentration (S. Brenner, S. Hay & N. S. Scrutton, unpublished data). Therefore, the buffer system used was MTE (see Materials and methods), which allows the analysis of the pH dependence of the reaction without changing the ionic strength [40,41].

In the first series of stopped-flow experiments, oxidized CPR was mixed with a 20-fold excess of NADPH at 25 °C at pH 7.0 and 8.5 (Fig. 1A,B) and photodiode array (PDA) data were collected. Oxidized CPR shows a characteristic absorbance maximum around 454 nm and essentially no absorption at 600 nm (Fig. 1, spectra a). Over short timescales (10 s data acquisition), a decrease in absorbance is observed at 454 nm resulting from the reduction of the flavin cofactors. An initial increase in absorbance has been reported for the sq signature at 600 nm upon two-electron reduction, followed by the successive quenching of the sq signal upon further reduction to the three- and four-electron level [30]. (Data collection over long timescales results in an increase at 600 nm resulting from the establishment of the thermodynamic equilibrium between various reduction states [31].) At neutral pH, we collected PDA scans and confirmed the transient formation of the blue di-sq species (Fig. 1A, spectrum b). However, at pH 8.5 little absorbance at 600 nm was detected (Fig. 1B, spectrum b). The final reduction levels, as indicated by the decreasing absorbance at 450 nm, were comparable for both pH values (Fig. 1A,B, spectra c). The apparently diminished formation of the blue di-sq species at elevated pH may result from thermodynamic and/or kinetic variations in the reductive half-reaction at different pH values (Scheme 2). Possible thermodynamic reasons for this observation include the diminished formation of neutral, blue sq resulting from a shift towards the anionic, red sq species and/or from a shift towards the other two-electron reduced enzyme species shown in Scheme 1 (QE), namely $FMN_{ox}FAD_{hq}$ and $FMN_{hq}FAD_{ox}$. The loss in amplitude at 600 nm may also be due to a pH-dependent extinction coefficient of the neutral sq species. Kinetically, differences in the time separation of the up phase and the down phase at 600 nm might result in a poorer kinetic resolution at high pH yielding apparently less blue di-sq. Moreover,

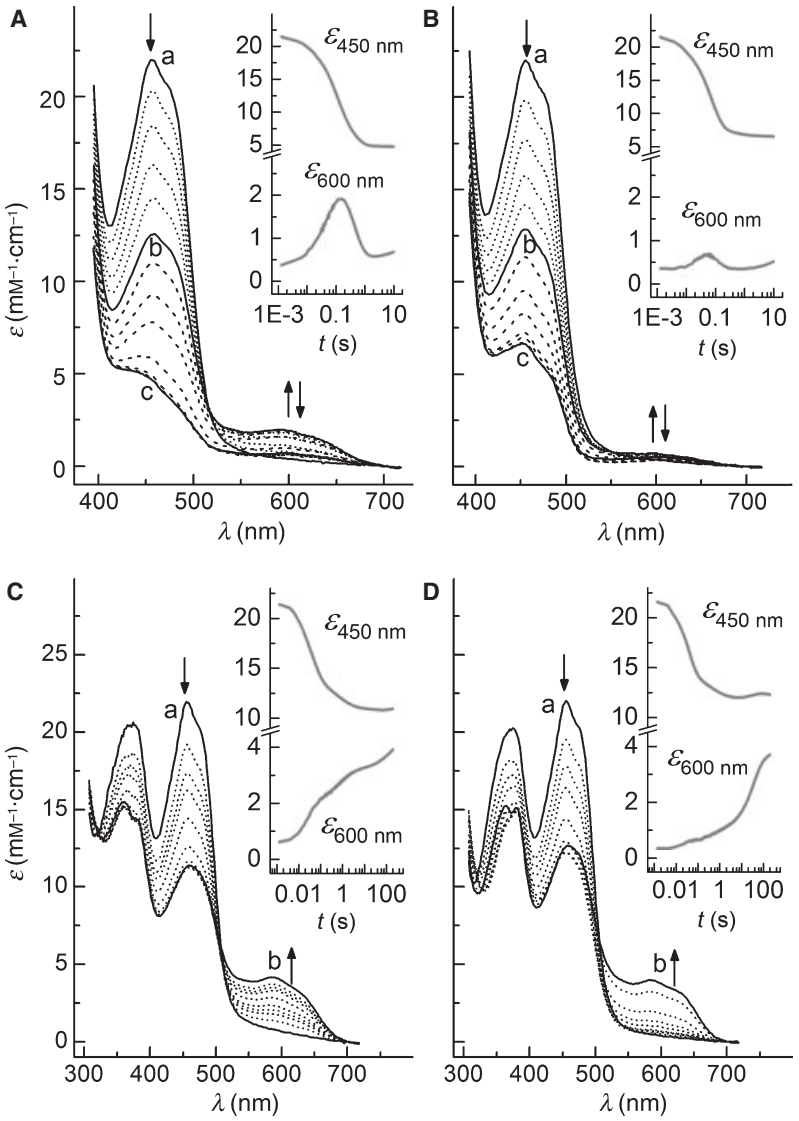

Fig. 1. Anaerobic stopped-flow diode array data collected upon mixing oxidized CPR with either a 20-fold excess of NADPH at pH 7.0 (A) and pH 8.5 (B) over 10 s or with stoichiometric amounts of NADPH at pH 7.0 (C) and pH 8.5 (D) over 200 s in MTE buffer at 25 °C. Selected spectra are shown in all panels. The arrows indicate the direction of absorption change upon CPR reduction. The solid lines in (A) and (B) reflect the oxidized enzyme (a), the mixture of partially reduced enzyme species (b) yielding maximum absorbance at 600 nm and the reduced CPR spectra (c), respectively; dotted and dashed lines represent selected intermediate spectra. The solid lines in (C) and (D) reflect the oxidized enzyme (a) and the thermodynamic mixture of two-electron reduced enzyme species (b) designated as QE in Scheme 1. Single-wavelength data extracted from the PDA files are shown as insets. The results of global analysis of the data in (A) and (B) are presented in Fig. S1 and for (C) and (D) in Fig. 5.

the blue di-sq species could be thermodynamically favourable but might not be accumulated during progression to the four-electron reduced state. These possibilities were explored using a combined thermodynamic and kinetic approach. Scheme 2 refers to those figures providing the relevant information for each of the listed possibilities.

To determine whether the anionic sq species is formed at high pH, stopped-flow PDA studies were performed, in which oxidized CPR was mixed with stoichiometric amounts of NADPH (Fig. 1C,D). Because of the overlapping absorbance of NADPH at 340 nm and the anionic sq at 380 nm, the anionic sq is only visible when CPR is reduced with stoichiometric amounts of NADPH (i.e. CPR : NADPH = 1 : 1). Because the dissociation constant of NADPH has been reported to be in the low μM region {K_i (2′,5′-ADP) = 5.4 ± 1.3 μM [33]; K_d (2′,5′-ADP) = 0.05 μM, K_d ($NADP^+$) = 0.053 μM, K_d ($NADPH_4$) = 0.07 μM [42]}, NADPH is expected to be completely bound to the enzyme under the conditions used in this experiment (30 μM final concentration). This reaction will then lead to the two-electron reduction of CPR. PDA data were acquired over long timescales (200 s) as a very slow absorbance increase at 600 nm was observed prior to the establishment of the apparent thermodynamic equilibrium of two-electron reduced enzyme species (Scheme 1, QE). At both pH 7.0 and pH 8.5, similar final levels of blue sq ($\varepsilon_{obs,\ 600\ nm} \sim 4 mM^{-1}·cm^{-1}$) were detected at 600 nm. (The protein concentration was determined for the oxidized enzyme using $\varepsilon_{454\ nm} = 22\ mM^{-1}\ cm^{-1}$. Observed absorbance

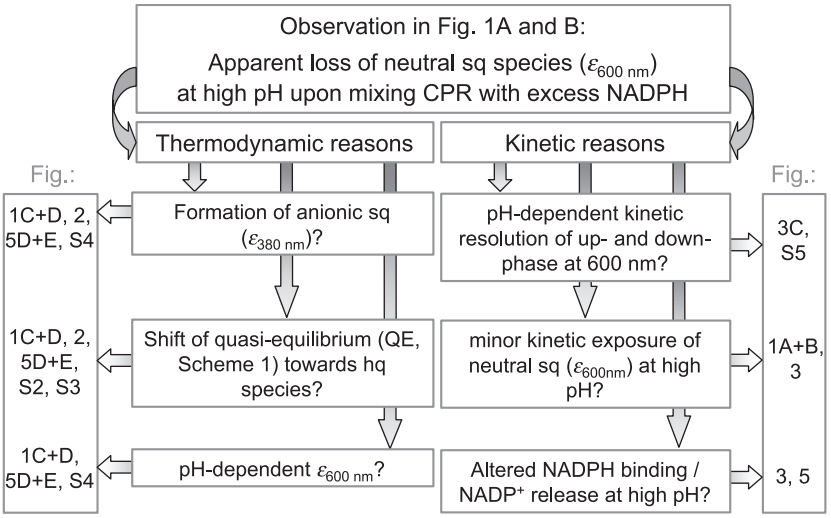

Scheme 2. Flow-chart (see text for further explanation).

changes were then converted into observed changes in ε using the known CPR concentration.) No significant absorption difference at 380 nm was observed at the two pH values. Thus, these preliminary experiments suggested that formation of the blue di-sq is equally favourable at neutral and basic pH values, and appreciable levels of the anionic sq species are not formed at either pH 7.0 or pH 8.5. Further, the thermodynamic equilibrium between the various two-electron reduced CPR species (Scheme 1) does not appear to be significantly altered by a pH change from 7.0 to 8.5 (see below).

Thermodynamic analysis of di-sq formation

Previous redox titrations [4,19] have revealed that the two-electron reduced enzyme exists in an equilibrium between the $FMN_{hq}FAD_{ox}$ and the $FMN_{sq}FAD_{sq}$ species, due to the similar redox potentials E_2 and E_3 for the two couples ($FMN_{sq} + e^- + H^+ \overset{E_2}{\rightleftharpoons} FMN_{hq}$ and $FAD_{ox} + e^- + H^+ \overset{E_3}{\rightleftharpoons} FAD_{sq}$). The corresponding equilibrium constant of $K_{298\ K} \sim 1$ at pH 7.0 was previously exploited to study the interconversion between these two two-electron reduced species kinetically using T-jump spectroscopy [33,34]. Thermodynamically, the loss in blue sq absorbance (Fig. 1A,B) could be explained by a shift in equilibrium towards the $FMN_{hq}FAD_{ox}$ species at elevated pH. However, this is not consistent with the stopped-flow data presented in Fig. 1C,D, where similar amounts of the di-sq species are formed at pH 7.0 and pH 8.5.

To confirm that the equilibrium between the two-electron reduced CPR species is unaffected by pH, additional redox titrations were conducted between pH 7.5 and 8.5 (25 °C). The data sets were evaluated by both single-wavelength analysis (Fig. S2), according to Munro *et al.* [19], and global analysis (as described for neuronal NOS [43]; Fig. S3). The previously published pH 7.0 data [19] were also re-evaluated using global analysis. The spectra recorded during the redox titration at pH 7.0 and 8.5 are shown in Fig. 2A,B, respectively. The insets in Fig. 2 show the extinction coefficient at 600 nm, reporting on the sq species [19], at varying solution potentials. Importantly, similar maximum absorbance values were observed at all pH values investigated. The overall course of the titration is shifted towards more negative potentials at elevated pH, consistent with a redox–Bohr effect. The assignment of the four midpoint reduction potentials in CPR is difficult [19], but the apparent change in redox potential with pH was confirmed by the values obtained from both global analysis using a Nernstian A ↔ B ↔ C ↔ D ↔ E model (Fig. S3B) and from multiple single-wavelength analysis (Fig. S2), as per Munro *et al.* [19]. A comparison between the four redox potentials (E_1–E_4) is given in Table 1 and the observed deviations are reasonable. However, the single-wavelength analysis was problematic for E_2, therefore, we feel that the globally analysed data set is preferable in interpreting the results.

The pH dependence of the redox potentials obtained by global analysis is presented in Fig. S3B and the four data sets were each fitted to a straight line. The slopes of the linear fits would be expected to be approximately $-59\ mV{\cdot}pH\ unit^{-1}$, for a 1-electron/1-proton process [44–46]. However, all four slopes were smaller than −59 mV, namely $-43 \pm 3\ mV{\cdot}pH^{-1}$ (E_1), $-17 \pm 18\ mV{\cdot}pH^{-1}$ (E_2), $-32 \pm 4\ mV{\cdot}pH^{-1}$ (E_3) and $-47 \pm 10\ mV{\cdot}pH^{-1}$ (E_4). The incomplete expression of the expected redox–Bohr effect may result from

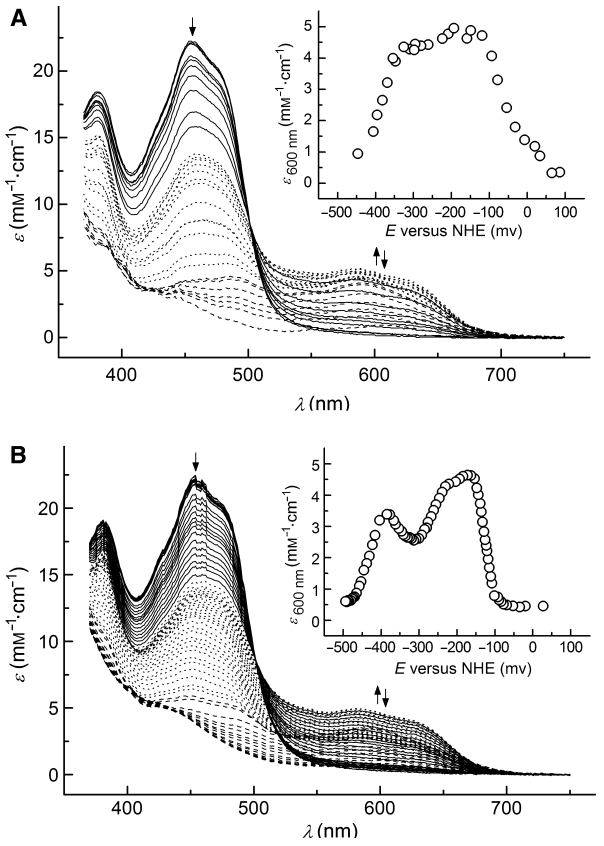

Fig. 2. pH-dependent anaerobic redox titration of CPR. (A) Representative titration recorded at solution potentials between +227 and −447 mV versus NHE in 100 mM KP_i, 10% (v/v) glycerol, pH 7.0 at 25 °C taken from Munro *et al.* [19] (for clarity not all data are shown). (B) Representative titration recorded at solution potentials between +36 and −494 mV versus NHE in 50 mM KP_i, pH 8.5 at 25 °C. The arrows indicate the direction of absorption change upon CPR reduction. The solid lines represent spectra recorded during the addition of the first electron with an isosbestic point at 501 nm (approximate isosbestic point for the ox/sq couples). The dashed lines indicate spectra with an isosbestic point around 429 nm (sq/red couples for both flavins) with the dotted lines being intermediate spectra. (Inset) Extinction coefficient changes at 600 nm versus solution potential (for clarity not all data points are shown).

errors in the estimation of the midpoint potentials. However, it is more likely that there is thermodynamic mixing of the species during potentiometric titration, i.e. the three intermediate species are not fully resolved [4,19,27], and, thus, the estimated midpoint potentials are not true microscopic reduction potentials. Considering the challenges in evaluating the presented redox potentiometry data, visual inspection of the *E* versus pH plot (Fig. S3B) may be adequate. The fits are parallel within error, implying that the equilibrium position between the $FMN_{hq}FAD_{ox}$ and the $FMN_{sq}FAD_{sq}$ species do not change greatly with pH. The pH dependence of the equilibrium constants $K_{298\ K}$, defined as $[FMN_{hq}FAD_{ox}]/[FMN_{sq}FAD_{sq}]$, were calculated using the difference in redox potentials ($E_2 - E_3$) of the corresponding redox couples (Table 1). The resulting values, between $K_{298\ K} \sim 11$ (pH 7.0) and $K_{298\ K} \sim 53$ (pH 8.5), showed a slight shift towards the FMN_{hq} FAD_{ox} species at higher pH values.

An anaerobic pH titration of CPR reduced to the two-electron level by NADPH (Fig. S4) confirmed a slight absorbance decrease at 600 nm upon raising the pH ($\varepsilon_{600\ nm} \sim 5 \cdot mM^{-1} \cdot cm^{-1}$ at pH 6.5 versus $\varepsilon_{600\ nm} \sim 3 \cdot mM^{-1} \cdot cm^{-1}$ at pH 8.5). No increase around 380 nm, which is indicative of an anionic sq species, was observed. Therefore, the subtle pH-dependent absorbance changes in the blue sq signature may reflect a minor shift in the equilibrium position between various two-electron reduced enzyme species (Scheme 1, QE) and/or slight variations in the extinction coefficients of the flavin semiquinones. However, this marginal change cannot account for the significant loss in amplitude at 600 nm during the kinetic experiments using excess NADPH (Fig. 1A,B). Thus, these redox titrations substantiate the stoichiometric stopped-flow experiments (Fig. 1C,D) in that the thermodynamic equilibrium is not significantly altered by changing the pH between 7.0 and 8.5.

Kinetic analysis of di-sq formation

Both the redox data and the pH titration of two-electron reduced CPR, discussed above, rule out any obvious thermodynamic reason for the pH-dependent variation in di-sq formation upon mixing oxidized CPR with excess NADPH. Therefore, the reaction was analysed at various pH values using stopped-flow spectrophotometry. The experiments presented below are analogous to the PDA studies presented in Fig. 1, except that single-wavelength measurements were performed to detect the blue sq signature at 600 nm and thus allow a more detailed kinetic analysis. Solvent and primary kinetic isotope effects were also investigated.

Oxidized CPR versus excess NADPH

In the first series of pH-dependent, single-wavelength stopped-flow experiments, oxidized CPR was mixed with a 20-fold excess of NADPH in MTE buffer at 25 °C. The experiment was performed in both H_2O and > 95% D_2O to determine the effect of solvent protons on the apparent rate of four-electron reduction. Consistent with observations in the PDA data

Table 1. Thermodynamic properties of CPR as a function of pH. Midpoint potentials (mV versus NHE) for the four-electron reduction of human CPR obtained by analysing the redox data by global (SVD) analysis as well as using single-wavelength (single-λ) analysis as described in the Materials and methods section. Redox titrations were performed at pH 7.5, 8.0 and 8.5. The data set at pH 7.0 has been published previously [19] and was re-analysed using global analysis. The assignment of E_1 and E_2 to the FMN and of E_3 and E_4 to the FAD cofactor, respectively, corresponds to the analysis of Munro *et al.* [19].

		FMN		FAD		$K_{298\ K}$[a]
pH		E_1	E_2	E_3	E_4	$[FMN_{hq}FAD_{ox}]/[FMN_{sq}FAD_{sq}]$
7	SVD	−72 ± 28	−221 ± 31	−288 ± 5	−388 ± 7	11 ± 1.4
	single-λ	−66 ± 8	−269 ± 10	−283 ± 5	−382 ± 8	1.7 ± 2.7
7.5	SVD	−87 ± 3	−208 ± 10	−310 ± 5	−403 ± 5	103 ± 0.3
	single-λ	−89 ± 1	−246 ± 4	−328 ± 2	−381 ± 7	23.7 ± 0.2
7.5 (+1 mM $NADP^+$)	single-λ	−95 ± 2	−219 ± 8	−331 ± 6	−342 ± 11	75.6 ± 0.3
8	SVD	−113 ± 1	−255 ± 3	−328 ± 2	−417 ± 3	16.8 ± 0.2
	single-λ	−114 ± 1	−261 ± 26	−366 ± 3	−385 ± 10	57.7 ± 0.7
8.5	SVD	−135 ± 2	−233 ± 5	−336 ± 3	−462 ± 6	53.4 ± 0.2
	single-λ	−133 ± 2	−251 ± 31	−380 ± 11	−419 ± 6	145.8 ± 0.8

[a] The difference between the redox potentials of E_2 ($FMN_{sq} + e^- + H^+ \overset{E_2}{\rightleftharpoons} FMN_{hq}$) and E_3 ($FAD_{ox} + e^- + H^+ \overset{E_3}{\rightleftharpoons} FAD_{sq}$) obtained by global analysis was used to calculate a difference in free energy ($\Delta G_{298\ K}$, Eqn 10), which yields the equilibrium constant $K_{298\ K}$ (Eqn 11).

(Fig. 1A,B), a characteristic double-exponential up–down behaviour was observed at 600 nm (Fig. 3A) [1,31]. Also, a very slow increase in $\varepsilon_{600\ nm}$ could be detected (data not shown), which was accounted for during data fitting by the incorporation of a sloping baseline to the double-exponential fitting function (Eqn 2; see Materials and methods for more details). This extremely slow process ($k_{obs} \sim 0.003 \cdot s^{-1}$ when fitted exponentially) might reflect the establishment of the thermodynamically most stable equilibrium between various redox species, because the redox potential of NADPH (−320 mV at pH 7.0, redox–Bohr effect approximately $-29.5\ mV \cdot pH^{-1}$) [47] does not favour the stable formation of the four-electron reduced enzyme (Table 1 and Fig. S3B) [1,4].

Over the analysed pH range of 6.5–8.5, the amplitudes of the fast up phase and slow down phase were equal within error (Fig. 3B). The amplitudes of the fast as well as the slow kinetic phase, however, decreased by an order of magnitude from pH 6.5 to 8.5. These diminishing amplitudes would be explicable if only a fractional amount of enzyme participated in the reduction at high pH value. The PDA spectra (Fig. 1A,B, global analysis in Fig. S1), however, revealed that the overall degree of reduction, as indicated by the absorbance peak around 454 nm, was similar for both pH values and, hence, cannot account for the ~ 10-fold difference in amplitudes at 600 nm. In addition to the effect of pH on the amplitudes, the observed changes in $\varepsilon_{600\ nm}$ were significantly larger in D_2O than in H_2O. This is evident in the traces in Fig. 3A. The pH dependence of the amplitudes of the up phase and down phase in Fig. 3B was analysed using Eqn (4), a single pK_a expression. The resulting apparent average pK_a values (p$K_{a,app}$) are 7.3 ± 0.1 in H_2O (p$K_{a,up}$ = 7.4 ± 0.2; p$K_{a,down}$ = 7.3 ± 0.1) and 7.2 ± 0.1 in D_2O (p$K_{a,up}$ = 7.2 ± 0.1; p$K_{a,down}$ = 7.2 ± 0.1), respectively. These values are expected to be the same within error, because the solution pH in D_2O was corrected using Eqn (1).

The significant pH-dependent behaviour of the amplitudes in Fig. 3B is not reflected in the observed rate constants (Fig. 3C). Across the analysed pH range, the mean values of k_{fast} (up phase) are ~ 20 ± 5 and ~ 7 ± 3·s^{-1} in H_2O and D_2O, respectively. The mean values of k_{slow} (down phase) are ~ 2.1 ± 0.4 and ~ 1.5 ± 0.2·s^{-1} in H_2O and D_2O, respectively. The values obtained in H_2O correspond well with the previously published data, considering the slight differences in the ionic strengths [30,31]. The relatively large variability in the observed rate constants for various pH values, as well as for repeated experiments, might be due to subtle changes in ionic strength, e.g. as a result of over-titrating during the pH adjustments. In contrast to the rate constants, the solvent kinetic isotope effect (SKIE) does show a slight decrease with increasing pH (Fig. 3D). The largest $SKIE_{kfast}$ of 5.1 ± 0.2 was observed at pH 6.75, whereas the smallest value (0.8 ± 0.1) was measured at pH 8.25. The data could be analysed using Eqn (4) yielding a pK_a of 7.8 ± 0.2. This trend indicates that solvent protons may play a more significant role in rate-limiting the fast phase at low (neutral) pH than at higher pH (> 8) where the SKIE is essentially 1. The SKIE for the slow rate constants ($SKIE_{kslow}$ = 1.6 ± 0.2), however, is approximately constant over the investigated pH range.

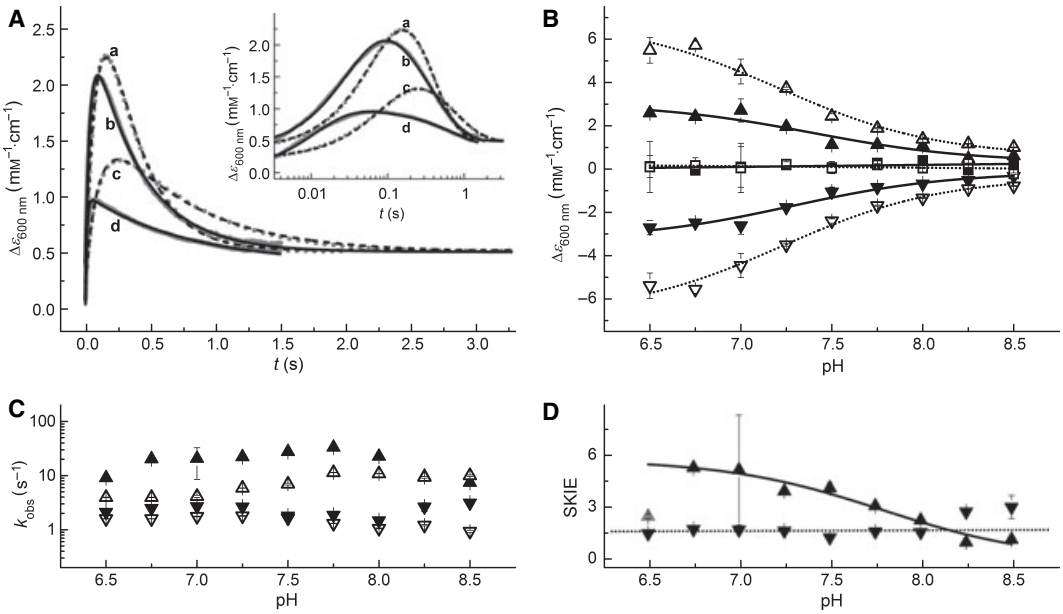

Fig. 3. Anaerobic stopped-flow data obtained by mixing oxidized CPR (30 μM final) with a 20-fold excess of NADPH in MTE buffer at 25 °C. Experiments were performed in H_2O (closed symbols) and D_2O (open symbols) at various pH values. Traces were recorded at 600 nm and analysed by a double-exponential equation plus sloping baseline (Eqn 2) yielding fast up-phases (up-triangles, k_{fast}) and slower down-phases (down-triangles, k_{slow}). (A) Representative stopped-flow traces (grey) in H_2O (solid lines) and D_2O (dashed lines) at pH 6.75 and 8.0 (a, D_2O pH 6.75; b, H_2O pH 6.75; c, D_2O pH 8.0; d, H_2O pH 8.0). The double-exponential fits to Eqn (2) are shown in black. Note that the traces are offset to yield the same final absorbance. The inset shows the same traces using a logarithmic timescale. (B) Amplitudes resulting from the double-exponential fit as a function of pH. The pH dependencies of the amplitudes of the up amplitudes and down amplitudes (triangles) were fitted to Eqn (4) (H_2O-fits, solid lines; D_2O-fits, dotted lines); the sums of the up amplitudes and down amplitudes are shown as squares and were fitted to a straight line. (C) The pH dependence of the observed rate constants for the up phase and down phase in H_2O and D_2O. The symbols are the same as those in (B). Figure S5 presents the ratio of k_{fast} and k_{slow} in H_2O and D_2O as a function of the pH value. (D) The pH dependence of the SKIEs for the up phase (up-triangles) and down phase (down-triangles). The data for k_{fast} (up phase) were fitted to Eqn (4) masking the data point at pH 6.5, whereas a linear fit was used for k_{slow} (down phase).

The effect of solvent-derived protons was further analysed by performing proton inventory experiments at pH 7.0 and 8.0. The solution pH in partially and completely deuterated buffer solutions was adjusted using Eqn (1). The ratio of the observed rate constant at a certain volume fraction of D_2O (n) (k_n) and the observed rate constant in pure H_2O (k_0) was plotted versus n (proton inventory plot, Fig. 4) and analysed using the simplified versions of the Gross–Butler equation (Eqns 5 and 6) [48]. The slow rate constants exhibited a clear linear behaviour at pH 7.0 and 8.0 in agreement with one solvent-exchangeable proton being (partly) rate-limiting. Accordingly, the data were analysed using Eqn (5). The measured $SKIE_{kslow}$ (k_{H2O}/k_{D2O}) values are 1.66 ± 0.05 at pH 7.0 ($p1$ = 0.60 ± 0.01) and 1.4 ± 0.04 at pH 8.0 ($p1$ = 0.704 ± 0.006), respectively. In contrast, and consistent with the difference in magnitude of the SKIEs, the behaviour of the fast rate constants differed for pH 7.0 and 8.0. Although a linear dependence was observed at pH 8.0 ($SKIE_{kfast}$ = 2.09 ± 0.02; $p1$ = 0.510 ± 0.008), the k_{fast} data show significant deviation from linearity at pH 7.0 (Fig. 4A) and were fitted to Eqn (6), accounting for two solvent-derived protons that contribute equally with $p1 = p2$ = 0.57 ± 0.01. These results substantiated the observed pH-dependent SKIE presented in Fig. 3D.

Both the pH dependence and the solvent dependence of the observed amplitudes might result from differences in the kinetic resolution, defined as the relative magnitude of two successive observed rate constants. Calculation of k_{fast}/k_{slow} revealed that the kinetic resolution is actually higher in H_2O than in D_2O (Fig. S5). Moreover, the ratio of k_{fast}/k_{slow} in either H_2O or D_2O did not exhibit the same pH-dependent trend as the amplitudes (compare Fig. 3B with Fig. S5). Hence, the kinetic resolution can account neither for the significant decrease in amplitudes with increasing pH nor for the differences in amplitudes in D_2O versus H_2O.

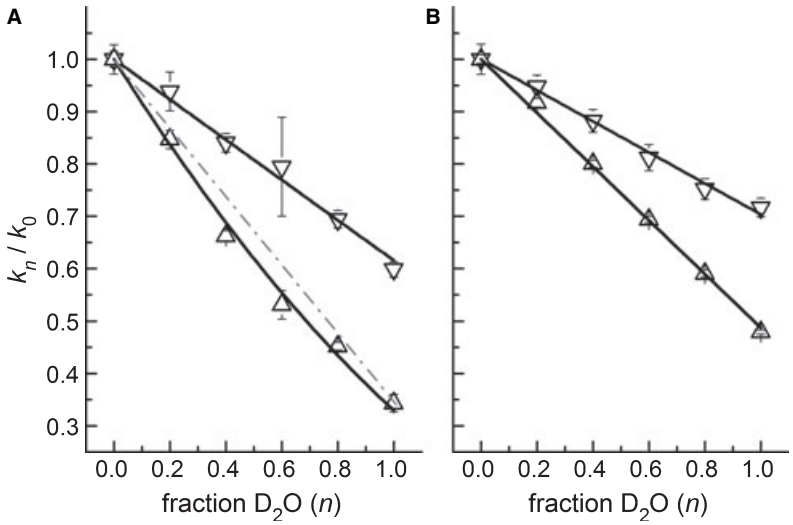

Fig. 4. Proton inventory stopped-flow experiments at pH 7.0 (A) and pH 8.0 (B) performed in MTE buffer at 25 °C. Oxidized CPR (30 μM final) was mixed with a 20-fold excess of NADPH. Traces were recorded at 600 nm and analysed as in Fig. 3 yielding fast up-phases (up-triangles) and slower down-phases (down-triangles). The ratio of the rate constant k_n, obtained at a certain fraction of D_2O (*n*), and the rate constant k_0 in pure H_2O was plotted against *n*. Linear fits to Eqn (5) are shown as solid lines for k_{slow} at pH 7.0 (down-triangles, A) and pH 8.0 (down-triangles, B) as well as for k_{fast} at pH 8.0 (up-triangles, B). The data for k_{fast} at pH 7.0 (up-triangles, A) were analysed using Eqn (6) (solid line); the dashed-dotted line is a straight connection between the data points at $n = 0$ and $n = 1$ demonstrating the curvature of this data set.

Oxidized CPR versus stoichiometric amounts of NADPH

To verify the qualitative result of the redox experiments, that the final equilibrium of the two-electron reduced enzyme species is largely independent of pH, further stopped-flow experiments were conducted, in which oxidized CPR was mixed with stoichiometric amounts of NADPH at various pH values (MTE buffer, 25 °C). PDA spectra (Fig. 1C,D) obtained upon the stoichiometric reduction of CPR with NADPH at pH 7.0 and 8.5 (Fig. 5) were analysed using a three-step W → X → Y → Z model (cf. the two-step model used above for the reduction of CPR by excess NADPH). The overall degree of reduction, given by the decreasing absorbance at 454 nm, is comparable for both pH values and essentially completed after the first two phases. By contrast, the absorbance changes at 600 nm differ substantially. At neutral pH, formation of blue di-sq occurs mainly during the first two phases, thus accompanying flavin reduction. At pH 8.5, however, the majority of the absorbance increase at 600 nm occurs during the third kinetic phase. This suggests that the thermodynamically unfavourable $FMN_{ox}FAD_{hq}$ species may accumulate at high pH because of a rate-limiting protonation. Another possibility may be that both electrons are transferred quickly from the FAD to the FMN cofactor yielding $FMN_{hq}FAD_{ox}$ without any accumulation of the di-sq species; the $FMN_{hq}FAD_{ox}$ may then relax back to the thermodynamic equilibrium position between this species and the blue di-sq. This alternative would also give an explanation for the lack of a clear isosbestic point in the pH 8.5 data, which is in contrast to the spectra collected at pH 6.5 with a reasonable isosbestic point around 501 nm.

Single-wavelength data at 600 nm were collected between pH 6.5 and 8.5 (Fig. 5). Consistent with the PDA data (Figs 1C,D and 5D,E), the thermodynamic equilibrium was reached very slowly, yielding triple-exponential traces over 1000 s and with all three amplitudes ($\Delta\varepsilon_1$–$\Delta\varepsilon_3$) leading to an increase in absorbance at 600 nm (Fig. 5A, Eqn 3). The relative amplitudes of the three resolved phases were significantly pH dependent with $\Delta\varepsilon_1$ and $\Delta\varepsilon_2$ decreasing at elevated pH and $\Delta\varepsilon_3$ correspondingly increasing (Fig. 5B). However, the overall amplitude change, and thus the final di-sq equilibrium position appears to be pH independent (Fig. 5B) – consistent with the redox potentiometry (Table 1). The data for D_2O collected at pH 7.0 and 8.5 have a similar overall amplitude as for H_2O (Fig. 5B), which is in contrast to the stopped-flow data acquired in the presence of excess NADPH. This indicates that the observed differences in amplitudes in Fig. 3 might have kinetic rather than thermodynamic origins. (Conducting redox titrations in a

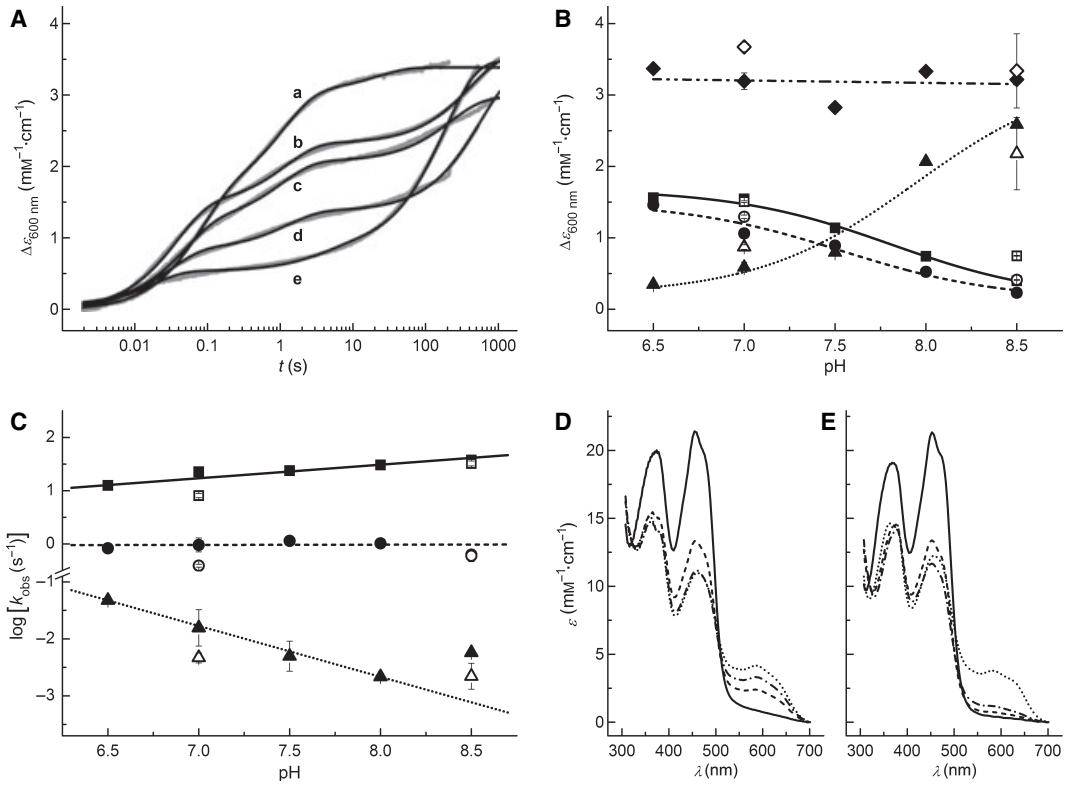

Fig. 5. Anaerobic stopped-flow data obtained by mixing oxidized CPR (30 μM final) with stoichiometric amounts of NADPH in MTE buffer at 25 °C. (A) Representative stopped-flow traces (grey) measured at 600 nm in H_2O for pH 6.5 (a), pH 7.0 (b), pH 7.5 (c), pH 8.0 (d) and pH 8.5 (e). All data were fitted to a 3-exponential function (Eqn 3; black lines). (B) The pH dependence of the three amplitudes observed: $\Delta\varepsilon_1$, squares; $\Delta\varepsilon_2$, circles; $\Delta\varepsilon_3$, triangles; $\sum_1^3 \Delta\varepsilon$, diamonds. Closed symbols are data points obtained in H_2O, while open symbols are the corresponding results in D_2O buffer. (C) The pH dependence of the three observed rate constants versus pH value: k_1, squares; k_2, circles; k_3, triangles. (D, E) Deconvoluted PDA spectral intermediates at pH 7.0 (D) and 8.5 (E) determined from a W → X → Y → Z model fit to the data in Fig. 1. The spectra are: solid lines, W; dashed lines, X; dashed-dotted lines, Y; dotted lines, Z. See text for more details.

deuterated buffer system would be rather complicated, because the electrode would have to be calibrated differently. We therefore refrained from doing these experiments.) Fitting the pH-dependent H_2O amplitudes to Eqn (4) gave p$K_{a,app}$ values of 7.8 ± 0.1 for the first, 7.5 ± 0.3 for the second and 7.9 ± 0.3 for the third phase, respectively. These values are within error of those obtained in the stopped-flow experiments using excess NADPH.

The pH dependence of the three observed rate constants is presented in a log-log plot (Fig. 5C). The faster rate constants k_1 and k_2 do not exhibit a significant pH-dependent behaviour, although the k_1 data do show a slight increasing trend with pH (k_1 = 12.6 ± 0.2·s^{-1} at pH 6.5 compared with k_1 = 37 ± 2·s^{-1} at pH 8.5). By contrast, the slowest rate constant k_3 decreased by a factor of 10 per pH unit and could be analysed using a linear fit, yielding a slope of dlog(k)/dpH = −0.89 ± 0.04. A slope of approximately −1 in the log-log plot is indicative of the rate-limiting transfer of one solvent-derived proton. Unfortunately, the available data do not allow the assignment of the chemical step (or steps) associated with k_3, but clearly this/these step(s) is/are largely rate-limited by proton binding. The effect of deuterated buffer on the observed rate constants showed a similar trend as observed during the four-electron reduction. All three rate constants exhibit an SKIE of 3 ± 0.3 at pH 7.0, yet only k_3 exhibits a significant SKIE of 2.6 ± 0.7 at pH 8.5.

Primary KIE using (R)-[4-^{2}H]-NADPH

Primary KIEs were used as a tool to assist in the deconvolution of the kinetic data in Figs 3 and 5. The primary KIE was first determined for the reaction of oxidized CPR with excess NAPDH in 50 mM KP_i (pH 7.5, 25 °C) yielding KIE values of 1.4 ± 0.1 and 1.3 ± 0.1 for the fast and the slow phase, respectively (data not shown). These relatively small primary KIEs

indicate that transfer of the hydride from NADPH to the FAD-N5 is probably not completely rate-limiting for either of the observed fast or slow rate constants. Previously, a KIE value of 3.4 has been reported for the fast phase in 50 mM Tris, pH 7.7, 28 °C [27] by monitoring flavin reduction at 452 nm. Therefore, it would appear that, although hydride transfer is partially, or fully, rate-limiting for the initial FAD reduction, hydride transfer is only marginally rate-limiting for the subsequent inter-flavin ET that forms the di-sq species observed at 600 nm.

To assist in the assignment of the three rate constants measured when oxidized CPR was mixed with stoichiometric amounts of NADPH (Fig. 5), the primary KIE was also determined in equivalent experiments at pH 7.0 and 8.0 at 25 °C in MTE buffer (Fig. S6). No KIE was measurable at pH 8.0 for any of the three kinetic phases (KIE_{k1} = 1.01 ± 0.05, KIE_{k2} = 0.8 ± 0.2, KIE_{k3} = 1.1 ± 0.2). At pH 7.0, only the first fast phase (k_1) exhibits a significant KIE (KIE_{k1} = 2.2 ± 0.2, KIE_{k2} = 1.0 ± 0.1, KIE_{k3} = 1.2 ± 0.2) indicating that the first rate constant of inter-flavin ET might be partially rate-limited by hydride transfer at pH 7.0, but not at pH 8.0. This observation substantiates the hypothesis that the kinetic mechanism, and thus the rate-limiting steps, changes between neutral and basic pH values. It would also appear that both k_2 and k_3 are not kinetically coupled to hydride transfer during the stoichiometric reduction of CPR with NADPH.

Summary of results

Scheme 2 outlines possible reasons for the diminishing intermediate formation of blue di-sq at increasing pH, when CPR is mixed with excess NADPH. In the following, a synopsis of the gathered results is used to support the hypothesis that the blue di-sq is kinetically less exposed at elevated pH.

The protonation state of the N5 in the flavin sq may depend on the solution pH and favour the formation of the anionic sq at elevated pH (Scheme 1). We can rule this out on the basis of a number of experiments. The total amount of neutral sq formed during the redox titrations does not change significantly with pH (Fig. 2, insets). The PDA raw data (Fig. 1C,D) and the globally analysed data sets (Fig. 5D,E) showed no increase in anionic sq absorbance at 380 nm at elevated pH. Further, a similar amount of neutral di-sq species is formed at pH 7.0 and 8.5 in the stopped-flow under single-turnover (stoichiometric) conditions (Fig. 5). As none of the experiments yielded any evidence for the formation of the anionic sq species, the apparent pK_a values observed in the stopped-flow experiments cannot be assigned to the deprotonation of the blue sq species. The crystal structure of CPR does not show any protonatable residues close enough to the flavin-N5 to serve as acid–base catalyst(s) [7,8]. The closest appropriate residues are located ~ 1 nm from the FMN-N5 (His180) and ~ 0.65 nm from the FAD-N5 (His319) and would have to undergo significant conformational transitions to adopt this role. Therefore, the observed pK_a probably reflects a macroscopic value, which may not result from any single amino acid residue. In light of the available data, a pH-dependent conformational change cannot be ruled out and further analysis is required to assist in the assignment.

The redox titrations revealed no significant pH-dependent shift in the equilibrium between various two-electron reduced redox species (Fig. 2 and Fig. S3; $FMNH^{\bullet}$,$FADH^{\bullet}$; FMN,$FADH_2$; $FMNH_2$,FAD; QE in Scheme 1). This was also confirmed by the similar final absorbance levels at 600 nm in the stoichiometric stopped-flow experiments. Thus, a shift towards the hq species is unlikely to be the reason for the changes in $\varepsilon_{600\ nm}$. Anaerobic pH titration of the two-electron reduced enzyme (Fig. S4) showed no increase in 380 nm absorbance at high pH; the slight increase in $\varepsilon_{600\ nm}$ at low pH cannot account for the 10-fold difference in the amplitudes at 600 nm observed upon mixing oxidized CPR with excess NADPH.

Kinetic analysis of the stopped-flow experiments in the presence of excess NADPH showed that the kinetic resolution of the fast up phase and the slow down phase at 600 nm is not decreased at high pH (Fig. 3 and Fig. S5). The rate constants for the depletion of the blue sq did not reveal a significant pH-dependence (Fig. 3C) indicating that $NADP^+$ release and the subsequent binding of a second NADPH molecule are unlikely to be significantly affected by pH. The stoichiometric PDA stopped-flow experiments (Fig. 5D,E) gave similar final levels of blue di-sq and comparable absorbance decreases at 454 nm implying that the K_d value of NADPH is sufficiently low to yield comparable reduction degrees within the investigated pH range. Moreover, flavin reduction (454 nm) accompanies the first two kinetic phases at 600 nm with relatively pH-independent rate constants (Fig. 5C), i.e. the rate of NADPH binding and hydride transfer to the FAD cofactor cannot account for the slow formation of blue di-sq during the third phase at high pH. In addition, this slow phase does not exhibit a primary KIE.

The three kinetic phases observed in the stoichiometric stopped-flow experiment appear to be kinetically complex and cannot be unequivocally assigned to individual reaction steps. However, these data may be interpretable by a pH-dependent relaxation towards the thermodynamic equilibrium between the three two-electron reduced species ($FMNH^{\bullet}$,$FADH^{\bullet}$; FMN,$FADH_2$; $FMNH_2$,FAD; QE in Scheme 1). The establishment of this thermodynamic equilibrium does not only become increasingly rate-limiting at high pH, as indicated by the pH dependence of the slowest phase (Fig. 5C), but also results in a redistribution of the total amplitude over the three kinetic phases at 600 nm. When an excess of NADPH is mixed with CPR, the relaxation to the thermodynamic equilibrium position of the two-electron reduced species competes with the reduction to the four-electron level by a second molecule of NADPH. Because the slow rate constants observed during the four-electron reduction are much faster than the slowest rate constant under stoichiometric conditions, the observed absorbance maximum at 600 nm only reflects a quasi-equilibrium position (cf. the thermodynamic equilibrium established under stoichiometric conditions). Thus, this hypothesis is consistent with the observation of an apparent decrease in the formation of blue di-sq with increasing pH upon four-electron reduction.

Additional evidence for a pH-dependent kinetic switch in the reductive half-reaction of CPR was provided by examining the solvent isotope effects on the two- and the four-electron reduction in the stopped-flow reactions. In both sets of experiments, the SKIE was found to be more pronounced at neutral than at basic pH. This was also confirmed by the proton-inventory experiments conducted for the four-electron reduction of CPR at pH 7.0 and 8.0 (Fig. 4). A further indication of the potential mechanistic switch is obtained by comparing the amount of di-sq formed during the reduction of CPR with both stoichiometric and excess NADPH. Although the levels of blue di-sq formation are similar in H_2O and D_2O in the stoichiometric experiments, the absorbance changes upon four-electron reduction are twice as large in D_2O across the pH range investigated. Although we are unsure of the precise mechanism behind these differences, these data provide another hint at the variable kinetic exposure of the blue di-sq in the presence of excess NADPH.

Discussion

During the last few years, detailed theoretical and kinetic studies have been undertaken to shed light on biological ET mechanisms revealing that a large proportion of these reactions are rate-limited by, or coupled to, adiabatic non-ET reactions [39]. The first case represents so-called 'gated' ET, in which a reaction preceding the actual ET event is much slower than the ET itself. In coupled ET reactions, the ET is actually rate-limiting, but follows a thermodynamically unfavourable fast equilibrium. Thus, the observed ET rate constant is a product of the true ET rate constant and the coupled equilibrium constant. For the enzyme studied here, human CPR, there is increasing evidence that the internal electron transfer between the FAD and the FMN cofactor may be gated by non-ET reactions including conformational transitions, product release and chemical gating steps (see above) [13,24,27,34,38]. The latter case may comprise rate-limiting hydride transfer from NADPH to FAD and (de)protonation events – i.e. pH gating.

To analyse the effect of pH on the inter-flavin ET during the reductive half-reaction in CPR, we performed pH-dependent redox potentiometry as well as detailed stopped-flow studies under various pH and solvent conditions. When NADPH was mixed rapidly with an excess of NADPH, neither the rate constant of di-sq formation nor the rate constant of the subsequent sq depletion was found to exhibit significant pH dependence. This observation implies that direct pH-gating, as observed for the slowest rate constant in a stoichiometric experiment, is unlikely to play a significant role during the four-electron reduction. Moreover, this result is not consistent with inter-flavin ET itself being gated by a rate-limiting (de)protonation to/from the solvent, as the four-electron reduction has to pass through the di-sq species. The measured SKIEs, however, indicate the relevance of solvent-exchangeable protons. Hydride transfer from the NADPH was found to be partially rate-limiting during the four-electron reduction at both neutral and elevated pH, whereas only the first kinetic phase at pH 7.0 exhibits a primary KIE during the stoichiometric stopped-flow experiment. The most significant finding of this study is the pH-dependent kinetic exposure of the blue sq upon four-electron reduction.

Related diflavin enzymes, such as methionine synthase reductase (MSR) and NOS, have been extensively analysed using both thermodynamic and kinetic techniques [1,43,49–58]. In human MSR as well as neuronal NOS (nNOS), the blue sq species has been found to be a thermodynamic intermediate during redox titrations [53,56,58]. However, PDA data collected for both enzymes established that it is not kinetically accumulated upon four-electron reduction

[53,57]. The reaction of MSR with stoichiometric amounts of NADPH revealed that the thermodynamic equilibrium between various two-electron reduced enzyme species is acquired in a very slow process with an observed rate constant of $\sim 0.0044 \cdot s^{-1}$ [57]. This means that the relaxation occurred in a similar order of magnitude as the slowest rate constant (k_3) detected for CPR in the presented stoichiometric experiments ($k_3 \sim 0.05 \cdot s^{-1}$ at pH 6.5 and $\sim 0.002 \cdot s^{-1}$ at pH 8.0). For MSR and NOS, the release of $NADP^+$ following the first hydride transfer has been proposed to rate-limit the ET between the flavin cofactors [53,57]. This explanation has been underpinned by the differences in amino acid sequence between CPR and nNOS. Whereas Trp676 is thought to facilitate $NADP^+$ release in human CPR [29], the analogous residue Phe1395 in nNOS [59] has been postulated to be less efficient in fulfilling this role [53,57]. In the case of MSR, however, the analogous residue is also a tryptophan (Trp697) and the proposed slow $NADP^+$ release was argued to be due to a greater conformational flexibility of the MSR active site [57]. A rate-limiting $NADP^+$ release is, however, inconsistent with our data obtained with CPR (see above, Summary of results). Other diflavin enzymes, e.g. bacterial flavocytochrome P450-BM3 (BM3) and its homologues, do not show any significant amounts of the neutral, blue FMN_{sq}, but rather form the anionic, red sq species [60]. In the case of BM3, this has been proposed to result from the unusual FMN binding site in the enzyme, where no stabilising hydrogen bond can be formed between the protonated FMN-N5 and the protein backbone (cf. the case in CPR) [8]. Our experiments on human CPR did not provide any evidence for the formation of the anionic sq species over the investigated pH range 6.5–8.5.

The physiological role of CPR as a link between the two-electron donor NADPH and the one-electron acceptors, the cytochromes P450, has been widely discussed in the literature. However, it is still a matter of debate, which CPR species – the FMN_{hq} or the FMN_{sq} – serves as electron donor [16]. Moreover, it is contentious whether CPR is reduced to the two-, three- or four-electron form during catalytic turnover, and various models have been proposed for the redox cycle. These uncertainties mainly arose from inconsistencies between steady-state reduction rates observed with cytochrome *c* as the electron acceptor and pre-steady-state rate constants measured for the reductive half-reaction of CPR. Whereas k_{cat} values between 12 and $48 \cdot s^{-1}$ have been reported for intact human CPR and of up to $80 \cdot s^{-1}$ for the enzyme missing the membrane anchor [16], inter-flavin ET rates of 20 and $3 \cdot s^{-1}$ have been published for the two- and four-electron reduction, respectively [30]. Therefore, it was postulated that the second inter-flavin ET leading to the four-electron reduced species is unlikely to have any biological significance. However, it has to be suggested that while most steady-state analyses have been performed using cytochrome *c* as artificial electron acceptor, studies using reconstituted systems yielded lower k_{cat} values [16]. Most strikingly, we have observed a large ionic strength (*I*) dependence of the ET reaction (S. Brenner, S. Hay & N. S. Scrutton, unpublished data) yielding rate constants of $\sim 100 \cdot s^{-1}$ for the two-electron and $\sim 5 \cdot s^{-1}$ for the four-electron reduction (298 K, $I = 630$ mM). Thus, slight differences in the experimental buffers used in this work might be sufficient to account for the discrepancies. Because electrons have to pass from the FAD to the FMN cofactor to be transferred to the P450 redox partner, at least the first inter-flavin ET is of biological relevance.

Conclusion

The data presented on human CPR indicate that the formation of the blue di-sq, and thus inter-flavin ET, is not functionally gated by proton transfer. Rather, it is the relaxation to the thermodynamic equilibrium position between various two-electron reduced enzyme species, which is affected by both the pH value and the solvent and which decelerates with increasing pH, i.e. is pH-gated. In the presence of excess NADPH, the thermodynamic equilibrium between the blue di-sq and other two-electron reduced species is established to a diminishing degree, as the solution pH is increased above neutral. This results in a minor kinetic exposure of the blue di-sq species upon four-electron reduction, while leaving the observed rate constants largely unaffected by pH. The findings at high pH mirror the general behaviour of the related enzymes MSR [55–58] and nNOS [53], in which the formation of blue sq species can only be observed thermodynamically but not as kinetic intermediates upon four-electron reduction. Therefore, the kinetic accumulation of the blue di-sq in CPR at neutral pH might be an exception rather than the rule within this family of diflavin enzymes. Moreover, the presented analyses highlight the kinetic complexity in CPR, which may be underestimated when studying the enzymatic mechanism only at neutral pH. The possibility of conformationally gated ET as well as the nature of the presented kinetic switch in the reductive half reaction of CPR should be explored in future studies on this important enzyme family.

Materials and methods

Anaerobic experimental conditions, CPR purification and sample preparation

All experiments were conducted in a Belle Technology (Portesham, UK) glove-box under a nitrogen atmosphere. Buffers were made anaerobic by bubbling with nitrogen for at least 20 min and transferred into the glove-box; the bottles were then left open in the glove-box overnight to achieve complete equilibration with the anaerobic atmosphere. Oxygen levels were kept below 2 p.p.m. throughout the experiment.

Intact human CPR was purified essentially as described previously [6,19]. The enzyme was purified in a partially reduced form and had to be oxidized prior to each experiment by adding a few grains of the oxidant potassium ferricyanide (Sigma, Poole, UK). This was performed within the anaerobic box. The protein solution was applied immediately onto a Pharmacia (Leatherhead, UK) PD-10 gel filtration column pre-equilibrated with the desired anaerobic buffer. Thus, this step resulted in the removal of ferricyanide as well as achieving the transfer of CPR into the required anaerobic buffer system. The CPR concentration was then determined using an extinction coefficient of $\varepsilon_{454\ nm} = 22 \cdot mM^{-1} \cdot cm^{-1}$ for the oxidized enzyme [30].

(*R*)-[4-^{2}H]-NADPH was prepared as described previously [61]. The ratio of the rate constants obtained using NADPH (k_H) and (*R*)-[4-^{2}H]-NADPH (k_D) gives the kinetic isotope effect (KIE) for the reaction: KIE = k_H/k_D.

Stopped-flow experiments

Stopped-flow experiments were performed under anaerobic conditions (see above) using an Applied Photophysics (Leatherhead, UK) SC18MV stopped-flow instrument. For all stopped-flow experiments, a final CPR concentration of 30 μM was used. CPR was either mixed with stoichiometric amounts or a 20-fold excess of NADPH (Melford Laboratories, Ipswich, UK). The concentration of NADPH was determined using an extinction coefficient of $\varepsilon_{340\ nm} = 6.22 \cdot mM^{-1} \cdot cm^{-1}$. The pH dependence of the CPR reduction by stoichiometric amounts of NADPH or (*R*)-[4-^{2}H]-NADPH and by excess NADPH was studied in MTE buffer (50 mM Mes, 25 mM Tris, 25 mM ethanolamine; Sigma) at 25 °C. The primary KIE of the reaction using excess NADPH was studied in 50 mM potassium phosphate (KP_i; Fisher Scientific, Loughborough, UK), pH 7.5.

SKIE studies and proton inventory experiments

The pH dependence of CPR reduction by NADPH was also analysed in MTE buffer prepared using D_2O (Goss Scientific, Great Baddow, UK) as solvent. Because of H_2O traces present in the buffer components, the final D_2O content was ~ 95%. The pH value was determined using a conventional pH meter and the pH reading (pH_{obs}) was corrected using:

$$\begin{aligned} pH_{obs} &= pH_{desired} - (\Delta pH)_n \\ &= pH_{desired} - (0.076 \cdot n^2 + 0.3314 \cdot n) \end{aligned} \quad (1)$$

where $(\Delta pH)_n$ is a correction factor depending on the volume fraction of D_2O (n), i.e. $n = 1$ for pure D_2O [48,62]. Proton inventory experiments, in which the amount of D_2O was varied from 0 to 100% (i.e. $0 \le n \le 1$), were also conducted in MTE buffer, using Eqn (2) to determine the corrected pH value. The ratio of the rate constants obtained in 100% H_2O (k_{H_2O}) and the rate constants in pure (~ 95%) D_2O (k_{D_2O}) gives the solvent kinetic isotope effect (SKIE) for the reaction: SKIE = k_{H_2O}/k_{D_2O}.

Evaluation of stopped-flow data

Single-wavelength data were evaluated using the software package ORIGIN (OriginLab, Northampton, MA, USA). Global analysis of the photodiode array data was performed using SPECFIT/32 (Kromatek, Great Dunmow, UK). Stopped-flow data collected when CPR was reduced with excess NADPH were measured at 600 nm and exhibited typical 'up–down' behaviour characteristic of the formation and subsequent depletion of the blue sq species of CPR. Over a long timescale the absorbance at 600 nm increased very slowly. Accordingly, single traces detected as absorbance changes were transformed into changes in extinction coefficient and fitted to a double-exponential equation with a sloping baseline, where the sloping baseline approximates the slow increase in absorbance:

$$\Delta\varepsilon_{600nm} = \varepsilon_0 - \Delta\varepsilon_{fast} \cdot \exp(-k_{fast} \cdot t) - \Delta\varepsilon_{slow} \cdot \exp(-k_{slow} \cdot t) + m \cdot t \quad (2)$$

where $\Delta\varepsilon_{600\ nm}$ is the change in extinction coefficient at 600 nm, ε_0 an offset value, $\Delta\varepsilon_{fast}$ the amplitude change related to the fast up-rate k_{fast}, $\Delta\varepsilon_{slow}$ the amplitude change related to the slow down-rate k_{slow}, and m the slope. We chose to fit this to a linear rather than to an exponential function, because the number of data points required for the resolution of the two fast phases excluded the use of the long acquisition times required to resolve the very slow third phase (at least 1000 s). The single-wavelength data obtained by mixing stoichiometric amounts of CPR and NADPH showed three up-phases at 600 nm and were analysed using a triple-exponential equation yielding the three rate constants k_1, k_2 and k_3 with the amplitudes $\Delta\varepsilon_1$, $\Delta\varepsilon_2$ and $\Delta\varepsilon_3$, respectively:

$$\begin{aligned} \Delta\varepsilon_{600nm} = \varepsilon_0 &- \Delta\varepsilon_1 \cdot \exp(-k_1 \cdot t) - \Delta\varepsilon_2 \cdot \exp(-k_2 \cdot t) \\ &- \Delta\varepsilon_3 \cdot \exp(-k_3 \cdot t) \end{aligned} \quad (3)$$

The pH dependence of the amplitudes was analysed using:

$$\Delta\varepsilon = (\Delta\varepsilon_{LHA} \cdot 10^{-pH} + \Delta\varepsilon_{LA} \cdot 10^{-pKa})/(10^{-pKa} + 10^{-pH}) \quad (4)$$

where $\Delta\varepsilon$ is the amplitude of a single kinetic phase; $\Delta\varepsilon_{LHA}$ and $\Delta\varepsilon_{LA}$ are the amplitudes of the protonated and deprotonated species, respectively. Proton inventory experiments were analysed by plotting the ratio of the rate constant k_n, obtained at a certain volume fraction of D_2O (n), and the rate constant k_0 in pure H_2O versus n. Where appropriate, the data were fitted linearly indicating that one proton may be involved in the reaction [48]:

$$k_n/k_0 = (1 - n - n \cdot p_1) \quad (5)$$

where p_1 is the inverse SKIE. The simplified Gross–Butler equation for two protons being involved [48] was used to fit curved data sets:

$$k_n/k_0 = (1 - n - n \cdot p_1) \cdot (1 - n - n \cdot p_2) \quad (6)$$

where p_1 and p_2 are the inverse SKIE for each site and the total SKIE results from [48]:

$$SKIE_{total} = (p_1 \cdot p_2)^{-1} \quad (7)$$

Anaerobic potentiometric titrations

Redox titrations were performed anaerobically in a Belle Technology glove-box under a nitrogen atmosphere as described previously [19,43,63]. CPR was oxidized and made anaerobic as described above. Potentiometric titrations were performed in 50 mM KP_i, pH 7.5, 8.0 and 8.5, respectively, using 5 mL of $\sim$ 50 μM CPR; the redox titration at pH 7.5 was also conducted in the presence of 1 mM $NADP^+$ (Melford Laboratories, Ipswich, UK). CPR was titrated electrochemically according to the method of Dutton [64] using sodium dithionite (Sigma) as reductant and potassium ferricyanide as oxidant at 25 °C. Redox mediators (0.3 μM methyl viologen, 1 μM benzyl viologen, 7 μM 2-hydroxy-1,4-naphthoquinone, 2 μM phenazine methosulphate; Sigma) were added to electrically mediate between the enzyme and the electrode at solution potentials between +100 and −480 mV versus the NHE [19]. A Hanna pH 211 meter coupled to a Pt/Calomel electrode (ThermoRussell Ltd., Auchtermuchty, UK) was used to detect the electrochemical solution potential and spectra were recorded using a Cary UV-50 Bio UV–Vis scanning spectrophotometer (Varian, Palo Alto, CA, USA). Between dithionite and ferricyanide additions, respectively, the electrode was allowed to equilibrate for at least 4 min, which was the time needed to reach an equilibrium position as concluded from consecutively collected spectra being unaltered. (The presence of mediators results in a short-circuit of any slow electron transfer. Therefore, the acquisition time of 1000 s used in some stopped-flow experiments, e.g. Fig. 5, cannot be used as a measure for the time needed to reach an equilibrium during a redox titration.) The electrode was calibrated using the Fe^{3+}/Fe^{2+} EDTA couple as standard (+108 mV) and the correction factor relative to the NHE was +244 mV. Redox data were evaluated using single-wavelength analysis as well as global analysis (SPECFIT/32). The latter was done using a Nernstian 4 × 1-electron A ↔ B ↔ C ↔ D ↔ E model. The single-wavelength analysis was performed using ORIGIN software as described previously [19]. The data were fit to:

$$\varepsilon = \frac{a \cdot 10^{(E-E_1)/59} + b + c \cdot 10^{(E_2-E)/59}}{1 + 10^{(E-E_1)/59} + 10^{(E_2-E)/59}} + \frac{d \cdot 10^{(E-E_3)/59} + e + f \cdot 10^{(E_4-E)/59}}{1 + 10^{(E-E_3)/59} + 10^{(E_4-E)/59}} \quad (8)$$

where ε is the total extinction coefficient at a certain wavelength, *a–c* are the component extinction coefficient values contributed by one flavin in the oxidized, semiquinone and reduced states, respectively, *d–f* are the corresponding values of the other flavin. The values of *a–f* were allowed to vary freely after giving reasonable estimates as starting values. E is the measured potential, E_1, E_2, E_3 and E_4 correspond to the midpoint potentials of ox/sq and sq/red couples of the two flavins, respectively. For the redox data set in the presence of $NADP^+$ another redox couple ($NADP^+$/NADPH) was added to the equation, since dithionite-reduced CPR can function to donate electrons to $NADP^+$:

$$\varepsilon = \frac{a \cdot 10^{(E-E_1)/59} + b + c \cdot 10^{(E_2-E)/59}}{1 + 10^{(E-E_1)/59} + 10^{(E_2-E)/59}} + \frac{d \cdot 10^{(E-E_3)/59} + e + f \cdot 10^{(E_4-E)/59}}{1 + 10^{(E-E_3)/59} + 10^{(E_4-E)/59}} + \frac{g + h \cdot 10^{(E-E_5')/29.5}}{1 + 10^{(E-E_5')/29.5}} \quad (9)$$

where g and h are the component extinction coefficients for $NADP^+$ and NADPH, respectively, and E_5 is the redox potential of the $NADP^+$/NADPH-couple. The reported error for both SVD analysis and single-wavelength analysis given in Table 1 are those resulting from the respective fitting procedure.

Differences in redox potentials (ΔE) are linked to changes in free energy (ΔG) via

$$\Delta G = -n \cdot F \cdot \Delta E \quad (10)$$

where n is the number of electrons involved and F the Faraday constant. The equilibrium constant K for the reaction is obtained by

$$K = \exp^{-\Delta G/(R \cdot T)} \quad (11)$$

where R is the gas constant and T the absolute temperature. The error bars for the equilibrium constant K were determined using standard error propagation.

Acknowledgements

We thank Ted King (TgK Scientific Ltd) for PhD studentship funding (SB). We also thank the UK Biotechnology and Biological Sciences Research Council for project grant support. NSS is a BBSRC Professorial Research Fellow. We also thank Michiyo Sakuma for skilled technical assistance and Dr Kirsty McLean for technical advice concerning redox potentiometry studies.

References

1 Iyanagi T & Mason HS (1973) Some properties of hepatic reduced nicotinamide adenine dinucleotide phosphate–cytochrome *c* reductase. *Biochemistry* **12**, 2297–2308.
2 Porter TD (1991) An unusual yet strongly conserved flavoprotein reductase in bacteria and mammals. *Trends Biochem Sci* **16**, 154–158.
3 Porter TD & Kasper CB (1986) NADPH–cytochrome P-450 oxidoreductase: flavin mononucleotide and flavin adenine dinucleotide domains evolved from different flavoproteins. *Biochemistry* **25**, 1682–1687.
4 Vermilion JL & Coon MJ (1978) Identification of the high and low potential flavins of liver microsomal NADPH–cytochrome P-450 reductase. *J Biol Chem* **253**, 8812–8819.
5 Vermilion JL & Coon MJ (1978) Purified liver microsomal NADPH–cytochrome P-450 reductase. Spectral characterization of oxidation–reduction states. *J Biol Chem* **253**, 2694–2704.
6 Smith GC, Tew DG & Wolf CR (1994) Dissection of NADPH–cytochrome P450 oxidoreductase into distinct functional domains. *Proc Natl Acad Sci USA* **91**, 8710–8714.
7 Hubbard PA, Shen AL, Paschke R, Kasper CB & Kim JJ (2001) NADPH–cytochrome P450 oxidoreductase. Structural basis for hydride and electron transfer. *J Biol Chem* **276**, 29163–29170.
8 Wang M, Roberts DL, Paschke R, Shea TM, Masters BS & Kim JJ (1997) Three-dimensional structure of NADPH–cytochrome P450 reductase: prototype for FMN- and FAD-containing enzymes. *Proc Natl Acad Sci USA* **94**, 8411–8416.
9 Miller RT & Hinck AP (2001) Characterization of hydride transfer to flavin adenine dinucleotide in neuronal nitric oxide synthase reductase domain: geometric relationship between the nicotinamide and isoalloxazine rings. *Arch Biochem Biophys* **395**, 129–135.
10 Sem DS & Kasper CB (1992) Geometric relationship between the nicotinamide and isoalloxazine rings in NADPH–cytochrome P-450 oxidoreductase: implications for the classification of evolutionarily and functionally related flavoproteins. *Biochemistry* **31**, 3391–3398.
11 Lu AY, Junk KW & Coon MJ (1969) Resolution of the cytochrome P-450-containing omega-hydroxylation system of liver microsomes into three components. *J Biol Chem* **244**, 3714–3721.
12 Masters BS, Baron J, Taylor WE, Isaacson EL & LoSpalluto J (1971) Immunochemical studies on electron transport chains involving cytochrome P-450. I. Effects of antibodies to pig liver microsomal reduced triphosphopyridine nucleotide-cytochrome c reductase and the non-heme iron protein from bovine adrenocortical mitochondria. *J Biol Chem* **246**, 4143–4150.
13 Phillips AH & Langdon RG (1962) Hepatic triphosphopyridine nucleotide-cytochrome *c* reductase: isolation, characterization, and kinetic studies. *J Biol Chem* **237**, 2652–2660.
14 Wada F, Shibata H, Goto M & Sakamoto Y (1968) Participation of the microsomal electron transport system involving cytochrome P-450 in omega-oxidation of fatty acids. *Biochim Biophys Acta* **162**, 518–524.
15 Williams CH Jr & Kamin H (1962) Microsomal triphosphopyridine nucleotide-cytochrome *c* reductase of liver. *J Biol Chem* **237**, 587–595.
16 Murataliev MB, Feyereisen R & Walker FA (2004) Electron transfer by diflavin reductases. *Biochim Biophys Acta* **1698**, 1–26.
17 Vermilion JL, Ballou DP, Massey V & Coon MJ (1981) Separate roles for FMN and FAD in catalysis by liver microsomal NADPH–cytochrome P-450 reductase. *J Biol Chem* **256**, 266–277.
18 Shen AL, Porter TD, Wilson TE & Kasper CB (1989) Structural analysis of the FMN binding domain of NADPH–cytochrome P-450 oxidoreductase by site-directed mutagenesis. *J Biol Chem* **264**, 7584–7589.
19 Munro AW, Noble MA, Robledo L, Daff SN & Chapman SK (2001) Determination of the redox properties of human NADPH–cytochrome P450 reductase. *Biochemistry* **40**, 1956–1963.
20 Sevrioukova IF & Peterson JA (1995) Reaction of carbon monoxide and molecular oxygen with P450terp (CYP108) and P450BM-3 (CYP102). *Arch Biochem Biophys* **317**, 397–404.
21 Sem DS & Kasper CB (1993) Interaction with arginine 597 of NADPH–cytochrome P-450 oxidoreductase is a primary source of the uniform binding energy used to discriminate between NADPH and NADH. *Biochemistry* **32**, 11548–11558.
22 Sem DS & Kasper CB (1993) Enzyme–substrate binding interactions of NADPH–cytochrome P-450 oxidoreductase characterized with pH and alternate substrate/inhibitor studies. *Biochemistry* **32**, 11539–11547.
23 Sem DS & Kasper CB (1994) Kinetic mechanism for the model reaction of NADPH–cytochrome P450 oxidoreductase with cytochrome c. *Biochemistry* **33**, 12012–12021.

24 Sem DS & Kasper CB (1995) Effect of ionic strength on the kinetic mechanism and relative rate-limitation of steps in the model NADPH–cytochrome P450 oxidoreductase reaction with cytochrome c. *Biochemistry* **34**, 12768–12774.
25 Shen AL, Christensen MJ & Kasper CB (1991) NADPH–cytochrome P-450 oxidoreductase. The role of cysteine 566 in catalysis and cofactor binding. *J Biol Chem* **266**, 19976–19980.
26 Shen AL & Kasper CB (1995) Role of acidic residues in the interaction of NADPH–cytochrome P450 oxidoreductase with cytochrome P450 and cytochrome c. *J Biol Chem* **270**, 27475–27480.
27 Shen AL & Kasper CB (1996) Role of Ser457 of NADPH–cytochrome P450 oxidoreductase in catalysis and control of FAD oxidation–reduction potential. *Biochemistry* **35**, 9451–9459.
28 Shen AL & Kasper CB (2000) Differential contributions of NADPH–cytochrome P450 oxidoreductase FAD binding site residues to flavin binding and catalysis. *J Biol Chem* **275**, 41087–41091.
29 Gutierrez A, Doehr O, Paine M, Wolf CR, Scrutton NS & Roberts GC (2000) Trp-676 facilitates nicotinamide coenzyme exchange in the reductive half-reaction of human cytochrome P450 reductase: properties of the soluble W676H and W676A mutant reductases. *Biochemistry* **39**, 15990–15999.
30 Gutierrez A, Lian LY, Wolf CR, Scrutton NS & Roberts GC (2001) Stopped-flow kinetic studies of flavin reduction in human cytochrome P450 reductase and its component domains. *Biochemistry* **40**, 1964–1975.
31 Oprian DD & Coon MJ (1982) Oxidation–reduction states of FMN and FAD in NADPH–cytochrome P-450 reductase during reduction by NADPH. *J Biol Chem* **257**, 8935–8944.
32 Gutierrez A, Grunau A, Paine M, Munro AW, Wolf CR, Roberts GC & Scrutton NS (2003) Electron transfer in human cytochrome P450 reductase. *Biochem Soc Trans* **31**, 497–501.
33 Gutierrez A, Munro AW, Grunau A, Wolf CR, Scrutton NS & Roberts GC (2003) Interflavin electron transfer in human cytochrome P450 reductase is enhanced by coenzyme binding. Relaxation kinetic studies with coenzyme analogues. *Eur J Biochem* **270**, 2612–2621.
34 Gutierrez A, Paine M, Wolf CR, Scrutton NS & Roberts GC (2002) Relaxation kinetics of cytochrome P450 reductase: internal electron transfer is limited by conformational change and regulated by coenzyme binding. *Biochemistry* **41**, 4626–4637.
35 Marcus RA & Sutin N (1985) Electron transfers in chemistry and biology. *Bichim Biophys Acta* **811**, 265–322.
36 Moser CC, Keske JM, Warncke K, Farid RS & Dutton PL (1992) Nature of biological electron transfer. *Nature* **355**, 796–802.
37 Page CC, Moser CC, Chen X & Dutton PL (1999) Natural engineering principles of electron tunnelling in biological oxidation–reduction. *Nature* **402**, 47–52.
38 Bhattacharyya AK, Hurley JK, Tollin G & Waskell L (1994) Investigation of the rate-limiting step for electron transfer from NADPH:cytochrome P450 reductase to cytochrome b5: a laser flash-photolysis study. *Arch Biochem Biophys* **310**, 318–324.
39 Davidson VL (2002) Chemically gated electron transfer. A means of accelerating and regulating rates of biological electron transfer. *Biochemistry* **41**, 14633–14636.
40 Ellis KJ & Morrison JF (1982) Buffers of constant ionic strength for studying pH-dependent processes. *Methods Enzymol* **87**, 405–426.
41 Morrison JF & Stone SR (1988) Mechanism of the reaction catalyzed by dihydrofolate reductase from *Escherichia coli*: pH and deuterium isotope effects with NADPH as the variable substrate. *Biochemistry* **27**, 5499–5506.
42 Grunau A, Paine MJ, Ladbury JE & Gutierrez A (2006) Global effects of the energetics of coenzyme binding: NADPH controls the protein interaction properties of human cytochrome P450 reductase. *Biochemistry* **45**, 1421–1434.
43 Dunford AJ, Rigby SE, Hay S, Munro AW & Scrutton NS (2007) Conformational and thermodynamic control of electron transfer in neuronal nitric oxide synthase. *Biochemistry* **46**, 5018–5029.
44 Hay S, Westerlund K & Tommos C (2005) Moving a phenol hydroxyl group from the surface to the interior of a protein: effects on the phenol potential and p*K*(A). *Biochemistry* **44**, 11891–11902.
45 Pollegioni L, Porrini D, Molla G & Pilone MS (2000) Redox potentials and their pH dependence of D-amino-acid oxidase of *Rhodotorula gracilis* and *Trigonopsis variabilis*. *Eur J Biochem* **267**, 6624–6632.
46 Yalloway GN, Mayhew SG, Malthouse JP, Gallagher ME & Curley GP (1999) pH-dependent spectroscopic changes associated with the hydroquinone of FMN in flavodoxins. *Biochemistry* **38**, 3753–3762.
47 Hibberd DB & James AM (1984) *Dictionary of Electrochemistry*, 2nd edn. Macmillan, London.
48 Karpefors M, Adelroth P & Brzezinski P (2000) The onset of the deuterium isotope effect in cytochrome *c* oxidase. *Biochemistry* **39**, 5045–5050.
49 Abu-Soud HM & Stuehr DJ (1993) Nitric oxide synthases reveal a role for calmodulin in controlling electron transfer. *Proc Natl Acad Sci USA* **90**, 10769–10772.
50 Abu-Soud HM, Yoho LL & Stuehr DJ (1994) Calmodulin controls neuronal nitric-oxide synthase by a dual mechanism. Activation of intra- and interdomain electron transfer. *J Biol Chem* **269**, 32047–32050.
51 Daff S, Noble MA, Craig DH, Rivers SL, Chapman SK, Munro AW, Fujiwara S, Rozhkova E, Sagami I &

Shimizu T (2001) Control of electron transfer in neuronal NO synthase. *Biochem Soc Trans* **29**, 147–152.
52 Dunford AJ, Marshall KR, Munro AW & Scrutton NS (2004) Thermodynamic and kinetic analysis of the isolated FAD domain of rat neuronal nitric oxide synthase altered in the region of the FAD shielding residue Phe 1395. *Eur J Biochem* **271**, 2548–2560.
53 Knight K & Scrutton NS (2002) Stopped-flow kinetic studies of electron transfer in the reductase domain of neuronal nitric oxide synthase: re-evaluation of the kinetic mechanism reveals new enzyme intermediates and variation with cytochrome P450 reductase. *Biochem J* **367**, 19–30.
54 Miller RT, Martasek P, Omura T & Siler Masters BS (1999) Rapid kinetic studies of electron transfer in the three isoforms of nitric oxide synthase. *Biochem Biophys Res Commun* **265**, 184–188.
55 Olteanu H, Wolthers KR, Munro AW, Scrutton NS & Banerjee R (2004) Kinetic and thermodynamic characterization of the common polymorphic variants of human methionine synthase reductase. *Biochemistry* **43**, 1988–1997.
56 Wolthers KR, Basran J, Munro AW & Scrutton NS (2003) Molecular dissection of human methionine synthase reductase: determination of the flavin redox potentials in full-length enzyme and isolated flavin-binding domains. *Biochemistry* **42**, 3911–3920.
57 Wolthers KR & Scrutton NS (2004) Electron transfer in human methionine synthase reductase studied by stopped-flow spectrophotometry. *Biochemistry* **43**, 490–500.
58 Olteanu H, Munson T & Banerjee R (2002) Differences in the efficiency of reductive activation of methionine synthase and exogenous electron acceptors between the common polymorphic variants of human methionine synthase reductase. *Biochemistry* **41**, 13378–13385.
59 Zhang J, Martasek P, Paschke R, Shea T, Siler Masters BS & Kim JJ (2001) Crystal structure of the FAD/NADPH-binding domain of rat neuronal nitric-oxide synthase. Comparisons with NADPH–cytochrome P450 oxidoreductase. *J Biol Chem* **276**, 37506–37513.
60 Hanley SC, Ost TW & Daff S (2004) The unusual redox properties of flavocytochrome P450 BM3 flavodoxin domain. *Biochem Biophys Res Commun* **325**, 1418–1423.
61 Pudney CR, Hay S, Sutcliffe MJ & Scrutton NS (2006) Alpha-secondary isotope effects as probes of 'tunneling-ready' configurations in enzymatic H-tunneling: insight from environmentally coupled tunneling models. *J Am Chem Soc* **128**, 14053–14058.
62 Schowen KB & Schowen RL (1982) Solvent isotope effects of enzyme systems. *Methods Enzymol* **87**, 551–606.
63 McLean KJ, Scrutton NS & Munro AW (2003) Kinetic, spectroscopic and thermodynamic characterization of the *Mycobacterium tuberculosis* adrenodoxin reductase homologue FprA. *Biochem J* **372**, 317–327.
64 Dutton PL (1978) Redox potentiometry: determination of midpoint potentials of oxidation–reduction components of biological electron-transfer systems. *Methods Enzymol* **54**, 411–435.

Supporting information

The following supplementary material is available:
Fig. S1. Anaerobic stopped-flow PDA spectra obtained by mixing oxidized CPR (30 μM final) with a 20-fold excess of NADPH in MTE buffer pH 7.0 (A) and pH 8.5 (B), respectively, at 25 °C.
Fig. S2. Single-wavelength analysis of the redox titration in 50 mM KP_i, pH 7.5 at 25 °C (blue spectra in Fig. S3A).
Fig. S3. pH-dependent anaerobic redox titration of CPR.
Fig. S4. Anaerobic pH titration of CPR pre-reduced by stoichiometric amounts of NADPH.
Fig. S5. Anaerobic stopped-flow data obtained by mixing oxidised CPR (30 μM final) with a 20-fold excess of NADPH in MTE buffer at 25 °C (see Fig. 3).
Fig. S6. The primary KIE obtained in stopped-flow experiments.
Fig. S7. Anaerobic titration of oxidized CPR (black, 30 μM) with NADPH (solid lines) and dithionite (dashed lines) in 50 mM KP_i, pH 7.5 at 25 °C.
Table S1. Observed rate constants obtained from double-exponential fits to the anaerobic SF-data upon mixing CPR with a 20-fold excess NADPH in MTE buffer at 25 °C (see Fig. 3C).
Table S2. Observed rate constants obtained from double-exponential fits to the anaerobic SF-data upon mixing CPR with stoichiometric amounts of NADPH in MTE buffer at 25 °C (see Fig. 5C).

This supplementary material can be found in the online version of this article.

Please note: Blackwell Publishing are not responsible for the content or functionality of any supplementary material supplied by the authors. Any queries (other than missing material) should be directed to the corresponding author for the article.